Optical properties of the group-IV*B* refractory metal compounds

Anna Delin, Olle Eriksson, Rajeev Ahuja, and Börje Johansson
Condensed Matter Theory Group, Physics Department, Uppsala University, S-751 21 Uppsala, Sweden

M. S. S. Brooks
European Commission, European Institute for Transuranium Elements, Postfach 2340, D-76125 Karlsruhe, Germany

Thomas Gasche
Departamento de Física, Universidade de Aveiro, 3800 Aveiro, Portugal

Sushil Auluck
Department of Physics, University of Roorkee, Roorkee 247 667, India

J. M. Wills
Theoretical Division, Los Alamos National Laboratory, Los Alamos, New Mexico 87545
(Received 27 February 1996)

We have calculated *ab initio* the direct interband electric dipole transitions of the carbides, nitrides, and oxides of Ti, Zr, and Hf in the rocksalt structure using the full-potential linear muffin-tin orbital method. The dipole matrix elements are calculated explicitly. Our results are in extraordinarily good agreement with experiment. The optical spectra are analyzed and we explain the origin of the different structures in the spectra in terms of the calculated electronic structure. We also discuss the trends in the optical properties as the metal and nonmetal atom types are changed and how these trends relate to general concepts such as band filling, nuclear charge, and bandwidth. [S0163-1829(96)09927-4]

I. INTRODUCTION

The optical properties of a material have in general not been considered as a very useful tool for studying the electronic structure. The complication arises because dispersive energy bands are involved in both the initial and final states. The intricate dispersive behavior of the electron states makes it a formidable task to analyze the optical spectra and extract information about the underlying band structure. One way to get around this problem is to increase the energy of the photons and excite a core level. The interpretation of such experiments is easier since the process involves one dispersion-free state. However, in this process the core hole created distorts the original band structure, giving rise to features in the spectra that do not originate from the ground-state band structure. If the optical spectra could be calculated with sufficient accuracy, the possibility opens up of a detailed investigation of the electronic structure using low-energy photons. The lower the energy of the experimental probe, the less the system studied will be disturbed and the chance increases that we are actually looking at an electronic structure very close to the ground state.

Density functional theory states that the electronic ground state is a unique functional of the charge density.[1] The theory does not, however, say much about individual eigenvalues. In addition, the unoccupied eigenvalues above the Fermi energy do not contribute to the charge density. These eigenvalues are therefore completely absent in the functional. When calculating optical properties *ab initio* one identifies the calculated Kohn-Sham eigenvalues with quasiparticle excitations. If this approach can be proven to be successful for a wide range of systems, there is a clear indication that density functional theory has wider implications than the original theorems state. It would be highly desireable to have this extended validity on solid theoretical ground.

In this paper, we demonstrate that optical properties can indeed be calculated with high precision and thus be very useful for confirming or discarding a theoretical ground-state band structure. As an example, we have chosen the rocksalt structured carbides, nitrides, and oxides of titanium, zirconium, and hafnium. In addition, we discuss how the optical properties depend on band filling, anion (C, N, and O) atomic core charge, and cation (Ti, Zr, Hf) *d*-band width in an attempt to create a better understanding of which general features the electronic structure should exhibit for the material to have certain optical properties. There are several very recent publications, theoretical as well as experimental, devoted to the physical properties of especially the titanium compounds.[2–4] The main reason for the interest seems to be that these compounds constitute technologically important materials with a quite interesting electronic structure.

The carbides and nitrides of the transition metals, crystallizing in the rocksalt structure, are known as refractory metal compounds. The name stems from their high binding energies, resulting in high melting points and extreme hardness. In general, such properties are typical of materials that are covalently bonded. In addition to being very hard, the refractory metal compounds of Ti, Zr, and Hf exhibit metallic conductivities and optical properties comparable to those of the pure transition metals.[5] The crystal structure is, on the other hand, typical for ionic crystals. TiC is widely used in hard cutting tools and the nitrides exhibit solar selectivity.[6]

So far, to our knowledge there has been no calculation of the optical properties of these compounds that includes the full transition matrix elements. The calculation of optical properties requires, apart from the Kohn-Sham eigenvalues, the explicit use of the wave functions, which therefore should be described as accurately as possible. In the calculational method used here, we have gone beyond a minimal basis set using a so-called double basis (see below) and in addition no shape approximation of the potential is used.

Electronic band structure calculations of especially the titanium compounds have been performed by several authors.[2,4,7–10] Eibler, Dorrer, and Neckel,[11] have calculated the joint density of states for TiN and ZrN. In their calculation of the imaginary part of the dielectric function for the same compounds, they used an approximation for the transition matrix elements that does not take the radial part of the wave functions into account. A number of measurements of the optical properties of the nitrides have been performed.[12–16] Lynch *et al.*[17] have made measurements of the optical properties on substoichiometric TiC. Very recently, Gokhale, Barman, and Sarma[3] performed a systematic, experimental study of how the optical properties of TiO depend on the oxygen content.

II. DETAILS OF CALCULATIONS

A. Electronic structure

We have calculated the electronic structures self-consistently using the full-potential linear muffin-tin orbital (FP LMTO) method.[18] The calculations are based on the local density approximation to density functional theory, with the exchange-correlation potential parametrized according to Hedin and Lundqvist.[19] The full-potential method implies that the wave function, electron density, and potential are calculated without any geometrical approximation. Consider a general Bravais lattice with a basis consisting of atoms centered at positions **s**, in the primitive cell. The effective one-electron wave function can then be expressed as

$$\Psi(\mathbf{k},\mathbf{r}) = \sum_{a\mathbf{s}} c_{a\mathbf{s}} \sum_{\mathbf{T}} e^{i\mathbf{k}\cdot\mathbf{T}} \chi_a(\mathbf{r}-\mathbf{T}-\mathbf{s}), \tag{1}$$

where **k** is the crystal momentum and **r** the position in real space. The basis functions used here, $\chi_a(\mathbf{r}-\mathbf{T}-\mathbf{s})$, are called linearized muffin-tin orbitals (LMTO's).[20,21] The inner sum in Eq. (1) is over all Bravais lattice vectors **T**. The index $a=(nlm\kappa)$ is short for the quantum numbers and tail energies κ^2 involved.[20,21] The LMTO's are continuous and differentiable at the boundaries of the spheres centered at the atomic sites. In our implementation it is important that these spheres do not overlap. The ground-state energy eigenvalues and eigenfunctions are found by using the Rayleigh-Ritz variation method, which determines the expansion coefficients $c_{a\mathbf{s}}$ that give the lowest possible total energy. From this effective one-electron wave function, the density is calculated and a potential is constructed using Poisson's equation and the local approximation of the density functional. This potential is in turn used as input in the next iteration until self-consistency is reached.

The relative sizes of the muffin-tin radii are chosen as 3 to 2, with the larger sphere for the metal atom, implying that the muffin-tin spheres occupy 57% of the unit cell. All calculations are done at the experimental volume of the compound in question.[22] For the metal atoms, s, p, d, and f basis functions are used and for the nonmetal s, p, and d. The inclusion of the very high lying metal f and nonmetal d states improve the accuracy of the calculated optical spectra, but are superfluous in a ground-state band-structure calculation. A double basis set is used, i.e., two basis functions with the same quantum numbers connect to LMTO's with different tail energies. In an attempt to further improve on the quality of the calculated wave functions, we also make use of semicore p and s states for the metal atoms. These low-lying states are calculated using tail energies considerably lower than for the valence wave functions. However, they are allowed to hybridize fully with the valence states. The sampling of the irreducible wedge of the Brioullin zone (IBZ, in this case 1/48 of the full BZ) is done using the special k-point method.[23] In order to speed up the convergence of the k-point sampling, each eigenvalue is smeared with a Gaussian function of width 20 mRy. The ground-state electronic structure is calculated using 84 k points in the IBZ. In order to obtain convergence in the optical spectra, 364 k points in the IBZ are required. Of these, several are of high symmetry.

B. Optical properties

The optical properties of matter can be described by the complex transverse dielectric function $\epsilon(\mathbf{q},\omega)$ where **q** is the momentum transfer in the photon-electron interaction and ω is the energy transfer. At low energies one can set $\mathbf{q}=0$, and we arrive at the electric dipole approximation, which is assumed throughout this paper.

The crystal structure under consideration has cubic symmetry and for this special case $\epsilon(\omega)$ degenerates into a scalar. The real and imaginary parts of $\epsilon(\omega)$ are often referred to as ϵ_1 and ϵ_2, respectively.

In metals, there are two contributions to $\epsilon(\omega)$: intraband and interband transitions. The interband transitions can be further split into direct and indirect transitions. Both the intraband transitions and the indirect interband transitions must involve a third particle (e.g., a phonon) in addition to the electron and photon in order to account for the momentum transfer. These transitions are thus three-particle interactions, which considerably complicates a calculation from first principles. However, the intraband part of the dielectric function can be approximately modeled using the Drude formula:[24]

$$\epsilon^{\text{intra}}(\omega) = 1 - \frac{\omega_p^2}{\omega(\omega + i/\tau)}, \tag{2}$$

where ω_p is the free electron plasma frequency and τ is the relaxation time. These intraband transitions dominate at low energies and we will include them when comparing our results with experimental data. The indirect interband transitions are, at the current state of theoretical developement, not possible to calculate explicitly. However, we can expect them to add a rather smooth background to the spectra.[25]

The direct interband contribution to the imaginary part of the dielectric function, $\epsilon_2^{\text{inter}}$, is calculated by summing all possible transitions from occupied to unoccupied states, tak-

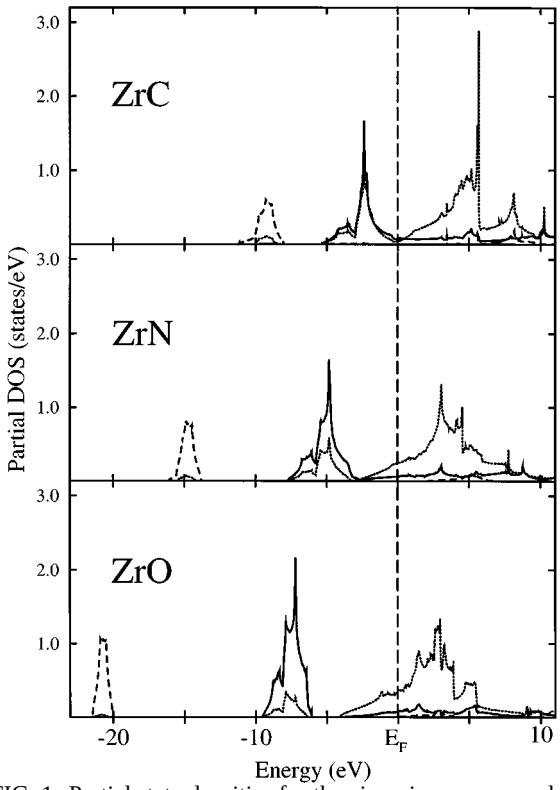

FIG. 1. Partial state densities for the zirconium compounds. The dashed, solid, and dotted curves are the partial *s*-, *p*-, and *d*-state densities, respectively. The Fermi energy is at zero. In the text, three main structures in the state densities are discussed. These are called the $2s$ peak, the $2p$ band, and the *d* band, respectively. The $2s$ peak is situated around -10 eV for the carbides, moving down to -22 eV for the oxides. The $2p$ band has a width of about 5 eV and extends up to the Fermi energy for the carbides whereas for the oxides it sits approximately 5 eV lower down. Finally, the *d* band is the wide structure above the broad minimum in the state density. For the carbides this structure is situated entirely above the Fermi energy. A decrease in *d* admixture in the $2p$ band is seen as the anion is changed from carbon to oxygen.

ing the appropriate transition matrix element into account.[26] The real part $\epsilon_1^{\text{inter}}$ is then determined from $\epsilon_2^{\text{inter}}$ by imposing the condition of causality.[27]

Finally, the complex optical conductivity $\sigma(\omega)$ is calculated using

$$\sigma(\omega) = -\frac{i\omega}{4\pi}\epsilon(\omega). \tag{3}$$

Using this definition,[28] the real part of the optical conductivity is essentially the imaginary part of the dielectric function scaled with the transition energy. In accordance with the notation for $\epsilon(\omega)$, the real part of the optical conductivity will be called σ_1 in the following.

III. RESULTS AND ANALYSIS

A. Electronic structure

Figure 1 shows the partial *s*-, *p*-, and *d*-state densities for the zirconium compounds. The corresponding state densities for the titanium compounds are very similar, except that the *d*-band width is smaller. The state densities for the hafnium compounds are extremely similar to the zirconium compounds. As we shall see, this similarity between the zirconium and hafnium compounds is reflected in the optical properties. Our state densities agree excellently with previous calculations,[2,4,7–10] especially for those without shape approximation of the potential.

The narrow structure centered at about -10 eV for ZrC is dominated by the energetically low-lying C $2s$ states and will therefore be called the $2s$ peak in the following. For ZrN and ZrO, the corresponding peaks are found around -15 and -22 eV, respectively. The decrease in energy of the $2s$ peak as the anion is changed from C to N to O reflects the increased nuclear charge, which results in contracted orbitals and lower-lying energy levels, but it is also an effect of band filling since all energies are relative to the Fermi energy.

In a simple view of the electronic structure, the metal *d* orbitals of e_g symmetry hybridize strongly with the *p* states of the nonmetal.[29,30] The double-peaked structure found between -6 eV and the Fermi energy for the carbides, a feature we loosely refer to as the $2p$ band, originates from the nonmetal $2p$ orbitals hybridizing with the metal *d* orbitals, as suggested. This hybridization is strongest for the carbides, weakening as the anion is changed, thus leading to a significantly smaller amount of *d* admixture in this structure for the oxides. This is clearly seen in the state density curves in Fig. 1 since for ZrC the $2p$ band is composed of an almost equal amount of $2p$ and *d* states, whereas for ZrO the $2p$ band is clearly dominated by the *p* orbitals. Further, the *d* contribution in the $2p$ band is of both e_g and t_{2g} symmetry with the e_g part dominating.[31] The corresponding $2p$ bands are found in the state densities for the nitrides between -8 and -3 eV and for the oxides between -11 and -7 eV. One recognizes the trend of decreasing energy from the discussion of the $2s$ peaks and the reasons for it should be the same as in that case. From the state density plots it is also apparent that the $2p$ peak narrows with increasing atomic number of the anion. This effect is due to core contraction.

The next structure encountered in the state densities as the energy is increased, has mostly *d* character originating from the metal, and is consequently called the *d* band. It is completely dominated by states with t_{2g} symmetry although there is an inmixing of *s* and *p* states.[31] This inmixing is crucial for the optical spectra. Since the width and center of mass of the *d* band increases with the main quantum number, n, due to orthogonality to the core states, we expect this structure to smear out and move upwards away from the Fermi energy as the metal is changed from Ti to Zr to Hf. This is indeed the case as can be seen from Fig 1. Also, the distance between the center of the $2p$ structure and the *d* band increases with the metal atomic number, which is entirely reasonable since the energy of an nd orbital with a high n quantum number must lie higher in energy with respect to an absolute level (e.g., the $2p$ orbital of C) compared to an nd orbital with a lower n.

The increased difference in energy between the $2p$ and the nd orbitals causes the hybridization to decrease when the nonmetal is changed from C to O. In the oxides the energy difference between the $2p$ and the nd orbitals is in fact so large that the intrinsic gap between the *p* and *d* bands remains in the solid.

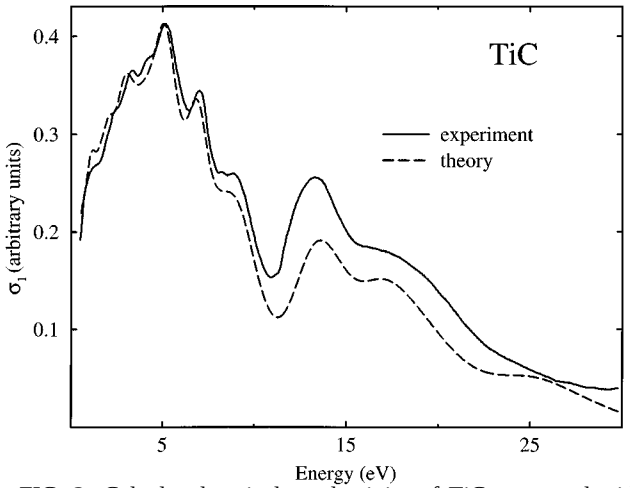

FIG. 2. Calculated optical conductivity of TiC compared with experiment. The solid curve is the experimental optical conductivity for $TiC_{0.90}$ calculated from reflectivity data (Ref. 17). The dashed curve is the present calculation. It has been broadened with a Gaussian distribution, whose width was taken to be 1/15 of the transition energy. A Drude term is included with $\omega_p = 10$ eV and $\tau = 0.3\ \mathrm{eV}^{-1}$. Its effect is to lift up the low-energy part of the spectrum. The relative amplitudes of the experimental and calculated spectra have been adjusted so that the maxima of the measured and calculated curves are the same.

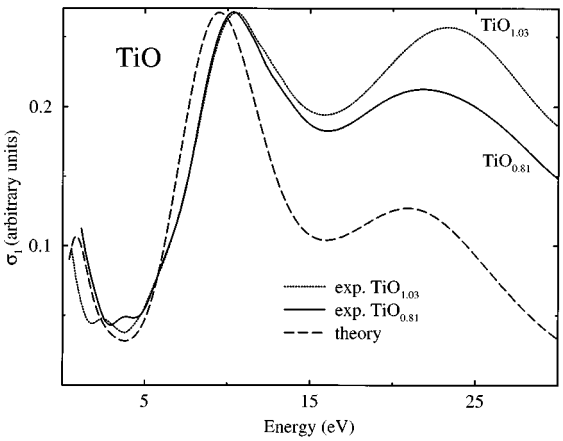

FIG. 3. Calculated optical conductivity of TiO compared with experiment. The solid and dotted curves are the experimental optical conductivities of TiO for two different stoichiometries calculated from electron energy loss spectra.[3] The dashed curve is the present calculation. It has been broadened with a Gaussian distribution, whose width was taken to be 1/7 of the transition energy plus a constant term in order to account for broadening due to randomly distributed vacancies. A Drude term is included with $\omega_p = 5$ eV and $\tau = 1\ \mathrm{eV}^{-1}$. Its effect is to lift up the low-energy part of the spectrum. The relative amplitudes of the experimental and calculated spectra have been adjusted so that the maxima of the measured and calculated curves are the same.

B. Optical properties

1. Comparison with experiment

In Fig. 2 the calculated real part of the optical conductivity for TiC is compared with experimental results obtained through measurements of the near normal reflectance. The spectrum contains a lot of structure and the agreement between our calculation and the measured spectrum is truly excellent. The positions of the local maxima and minima of the experimental curve are extremely well reproduced in the calculation, as are their relative amplitudes. The reasons for this are the very accurately described ground-state band structure and the explicit inclusion of the transition matrix elements. A calculation of the joint density of states, where the dipole matrix elements are all set to the same value, does not produce the correct relative peak intensities. The peak at 13 eV is due to carbon $s \rightarrow p$ and $p \rightarrow d$ transitions whereas the structure at 17 eV is dominated by carbon $p \rightarrow d$ transitions. Peaks at lower energies are discussed in more detail in the next section.

The same comparison is made for TiO in Fig. 3. Here, the experimental spectra are based on measurements of the electron energy loss. This spectrum has much less structure than the one for TiC. Again, the peaks are very well reproduced except the small bump around 2.5 eV (4 eV) for $TiO_{1.03}$ ($TiO_{0.81}$). Gokhale, Barman, and Sarma[3] attribute this bump to a plasmon loss, i.e., a longitudinal collective excitation of the electrons that cannot be activated using a transverse electric field. Our calculations show that the peak around 10 eV is due to O $p \rightarrow$ Ti d transitions, whereas the structure around 20 eV consists mostly of transitions from p to d states, where both the p and d states originate from the energy levels in oxygen. Transitions from the low-lying oxygen s bands to the p states just above the Fermi energy give a smaller contribution to this peak. We can thus confirm the interpretation made by Gokhale, Barman, and Sarma.[3]

Despite the generally very good agreement between the experimental and calculated conductivity spectra, some discrepancies do exist. The indirect interband transitions are not taken into account in the calculation and these can in part explain the tendency of the calculated spectra to decrease more rapidly towards higher energies than the experimental ones.[25] We observe that our calculation for stoichiometric TiO agrees better with the experimental spectrum of $TiO_{0.81}$ than it does with the spectrum of $TiO_{1.03}$. The stoichiometry quoted by Gokhale, Barman, and Sarma[3] was determined by measuring the increase in the weight of the samples on oxidation to TiO_2. Therefore, the numbers 0.81 and 1.03 only refer to the mean oxygen content of the samples and it may very well be the case that the surface of $TiO_{0.81}$ is closer to being stoichiometric than the surface of the $TiO_{1.03}$ sample. This offers an explanation as to why our calculation agrees better with the $TiO_{0.81}$ spectrum since the experimental method used (electron energy loss) is surface sensitive.

The position of the calculated 10-eV peak in the TiO spectrum is about 1 eV lower than in the experimental spectra. However, in the experiment by Wall, Ribarsky, and Stevenson,[32] the corresponding feature shows up slightly *below* 10 eV. The internal discrepancy between experiments is thus of the same order of magnitude as the difference between our calculation and any of these experiments.

Figure 4 shows measured and calculated reflectivities for TiN, ZrN, and HfN. The typical dip in the visible (for TiN) or UV (ZrN and HfN) region is excellently reproduced. However, the exact position of the dip is sensitive to one of the Drude parameters, as will be discussed in detail below. The minima in the reflectivity curves fall at 0.42 μm for TiN, 0.35 μm for ZrN, and 0.27 μm for HfN. The value of

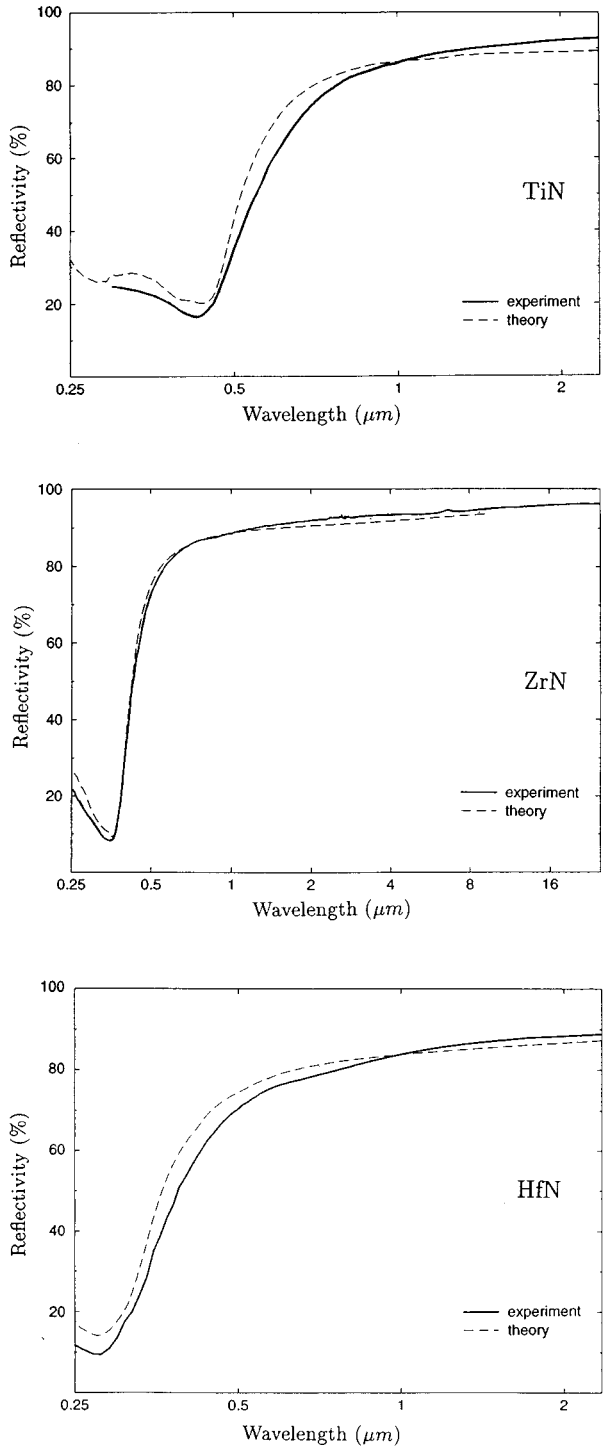

FIG. 4. Calculated and measured (Refs. 12–14) reflectivity spectra for the nitrides. The solid curves are measured reflectivities; the dashed curves are our calculated reflectivities. Note the different scale for ZrN. Drude parameters used were as follows: TiN, $\omega_p = 9$ eV and $\tau = 2.0\ \mathrm{eV}^{-1}$; ZrN, $\omega_p = 10$ eV and $\tau = 2.0\ \mathrm{eV}^{-1}$; HfN, $\omega_p = 12$ eV and $\tau = 1.0\ \mathrm{eV}^{-1}$.

the reflectivity at the minimum is seen to be around 20% for TiN and approximately 10% for the other two compounds. The behavior of the reflectivities, with a high reflectivity in the infrared, and transparency for shorter wavelenghts, make the nitrides very promising for solar control applications.[6] The low reflectance in the region of blue light for TiN creates the well-known goldlike color, so typical for this compound. Both ZrN and HfN have a more constant reflectance in the visible region ($\sim$0.4–0.8 μm) and are consequently more silverlike.

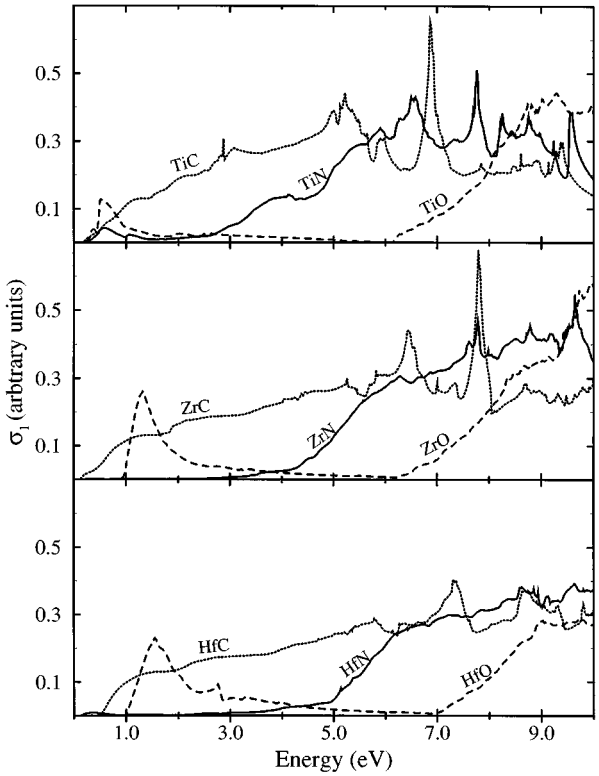

FIG. 5. Calculated real part of the optical conductivity. No broadening is applied. The solid curves are nitrides, the dotted carbides, and the dashed oxides.

From an experimental point of view, all the compounds considered in this paper are rather vacancy rich. For the carbides and nitrides, the vacancies are almost entirely situated on the anion sites. In the oxides the vacancies are equally distributed among both the metal and nonmetal sites. As a matter of fact, the experimental curve in Fig. 2 is for stoichiometry $TiC_{0.9}$ whereas the calculation is for the stoichiometric compound. The vacancies, if randomly distributed, will smear out sharp peaks and thus contribute to the broadening. They may also give rise to additional structures in the spectra. This is even more true for the TiO spectrum in Fig. 3. Although the excess number of oxygen atoms is small in the experimental sample, the number of vacant sites in the crystal is not.

2. Analysis of $\sigma_1^{inter}(\omega)$

We now turn to an analysis of the origin of the different structures in $\sigma_1^{\mathrm{inter}}$. This quantity is plotted for all nine compounds in Fig. 5 in the range 0–10 eV. In the corresponding spectra for $\epsilon_2^{\mathrm{inter}}$, the relative amplitudes of the low-energy structures will increase because ϵ_2 goes as σ_1/ω. In the $\sigma_1^{\mathrm{inter}}$ spectra, the energy dependence is thus partly scaled away, and it is revealed how the optical properties depend on the l characters of the bands involved. The nonmetal l states induce l states in the metal sphere and the metal l' states induce l' states in the nonmetal sphere. The direct dipole transitions take place between these induced states, most notably between p and d, and between s and p.

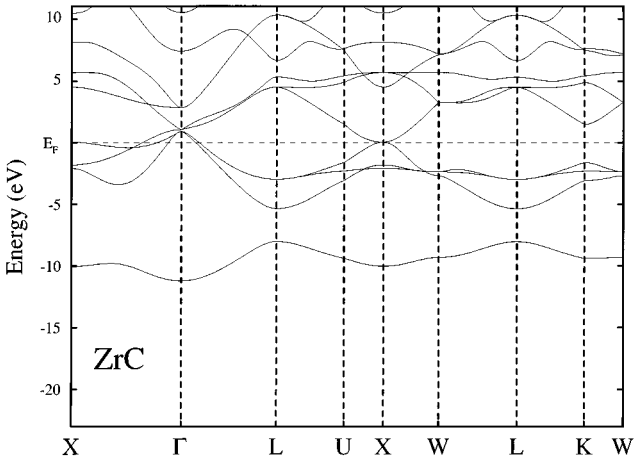

FIG. 6. Band structure for ZrC along the different symmetry lines of the Brillouin zone. Energy is in eV and the Fermi level is at zero.

Since $\sigma_1^{\text{inter}}(\omega)$ is a consequence of interband transitions, in order to analyze the details of the various peaks observed, it is of interest to investigate in detail the calculated energy band structure. For this reason we show in Figs. 6, 7, 8, and 9 the band structures for the zirconium compounds and also for TiN, since there are significant differences between ZrN and TiN.

There are in principle three main types of structures in the band structures that give rise to different features in the optical spectra: (a) close parallel bands crossing the Fermi level, (b) bands that are parallel in a significant part of the Brioullin zone, and (c) bands that are degenerate or close at one point and then separate from each other. The first type gives rise to bumps of interband transitions at low energies, the second type gives rise to peaks at higher energies, and the third type gives rise to an almost constant amount of interband transitions with a distinct onset energy. The term *bands* will be used here throughout although it would be more appropriate to discuss in terms of *eigenvalue surfaces* in reciprocal space. An eigenvalue at a general k point will have character from all angular momenta. At some high symmetry points, such as the X point, for instance, symmetry prohibits the mixing of even and odd angular momenta.

Starting with the carbides, we see that the real part of σ^{inter} in Fig. 5 is non-negligible already at energies as low as 0.5 eV. Thus, there is no free-electron-like region. The main contribution to σ_1^{inter} at very low energies comes from the two bands that are degenerate at X with an energy slightly larger than the Fermi energy. (For HfC they meet at an energy slightly lower than the Fermi energy.) The lower of these bands in the $[UX]$ and $[XW]$ directions belongs to the group of p bands, and its p character increases with the distance from X, whereas the higher of the two bands has mostly d character. The result is that the interband transitions start at a couple of tenths of eV for the carbides. As the bands move away from X, their energy separation diverges. Thus, this is a typical type (c) structure, which creates no sharp peaks but a flat constant contribution in the spectrum for σ_1^{inter}, which our explicit calculation of the individual contributions also shows. When the transition energy increases, more type (c) structures start to contribute. This creates the steady increase of σ_1^{inter}, which is a general feature of all spectra in Fig. 5. At about 5.2 eV for TiC, 6.5 eV for ZrC, and 7.2 eV for HfC, there is a semisharp peak. This is the maximum peak in the broadened spectrum in Fig. 2. In the region of $[UXW]$ in the band structure for the carbides, there are two parallel bands with the corresponding energy difference. The lower of these bands is the same band as the one giving rise to the low-energy transitions. The sharp peak at about 6.9 eV for TiC and 7.9 eV for ZrC is also clearly visible in the experimental spectrum for TiC (Fig. 2). It originates from transitions between two very flat bands that are parallel in the near surface region of the Brioullin zone. The lower of these bands is situated around -2.5 eV below the Fermi level and the higher around 5.5 eV. Both bands are visible as sharp peaks in the state density for ZrC; see Fig. 1. As the metal is changed from Ti to Hf the dispersion of the higher band increases, and this peak becomes smeared out and less pronounced, as seen in the spectrum for HfC.

The nitrides, in contrast to the carbides, have very little interband transitions at low energies and can be considered to be free-electron-like in that region. The small bump in the TiN spectrum at about 0.5 eV is due to the close and almost parallel bands that cross the Fermi level in $[\Gamma L]$; see Fig. 7. For TiN, these two bands are clearly separated and parallel

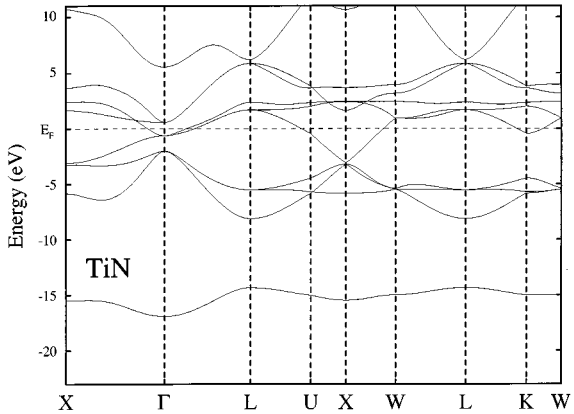

FIG. 7. Band structure for TiN along the different symmetry lines of the Brillouin zone. Energy is in eV and the Fermi level is at zero.

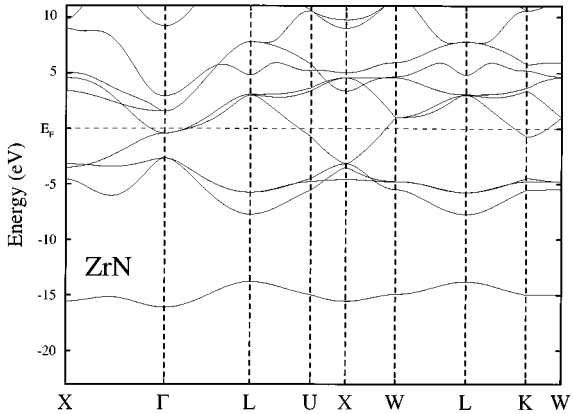

FIG. 8. Band structure for ZrN along the different symmetry lines of the Brillouin zone. Energy is in eV and the Fermi level is at zero.

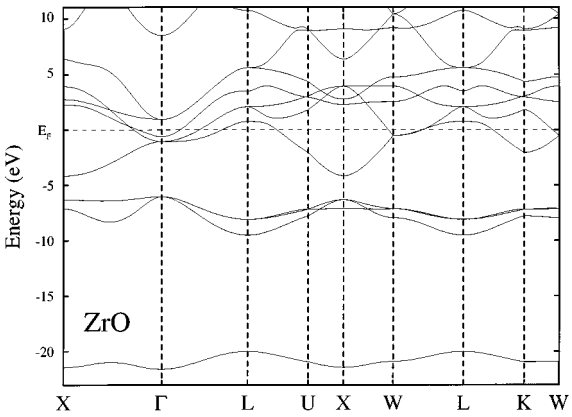

FIG. 9. Band structure for ZrO along the different symmetry lines of the Brillouin zone. Energy is in eV and the Fermi level is at zero.

near the Fermi level, in contrast to the situation for ZrN (Fig. 8). The corresponding but much smaller bump in the HfN spectrum has the same origin. These two bands are *d* dominated, as are all bands close to the Fermi level in the nitrides. This means that even if the bands are parallel, the amplitude of the transitions will not be high. The group of three bands centered around -5 eV are mostly of *p* character and when they become engaged in the transitions, σ_1^{inter} starts to increase rapidly. For all three nitrides, we see a slow onset of interband transitions, first visible only as tails in the spectra in Fig. 5. The tails are due to several structures centered around the Fermi level. The amplitude of the transitions is small because of the low *p* mixing in these bands. At 2.7 eV for TiN, 4.2 eV for ZrN, and 4.9 eV for HfN, the slope starts to increase more rapidly. This is because the *p* bands mentioned earlier become involved in the transitions. The minimum energy differences between these bands and an unoccupied band is at Γ and match exactly the energies quoted. At higher energies the main part of the transitions are still $p \rightarrow d$ but, as is apparent from Fig. 1, $p \rightarrow s$ transitions give a contribution since there is some inmixing of *s* states in the *d* peak above the Fermi level. In the nitride spectra we see the same sharp peaks as in the carbide spectra, although they are less pronounced compared to the carbides. As expected, the same bands are involved as in the carbides. The peaks are situated at higher energies, which is due to the increased energy difference between the *p* and *d* dominated bands. In Fig. 1 we see that the *d*-state density for ZrN has no very sharp peak in contrast to ZrC . This observation agrees entirely with the fact that the peaks in σ_1^{inter} are less sharp for the nitride than for the carbide.

The optical conductivity of the oxides shows a conspicuous peak at low energies, followed by a tail extending all the way up to about 6 eV for TiO and ZrO and around 7 eV for HfO. Then the big onset of interband transitions starts. The peak at low energy in TiO originates predominantly from the bands crossing the Fermi level in $[X\Gamma L]$; i.e., it is the same bands that cause the low-energy bump for TiN. For ZrN and HfN a band that is unoccupied in TiN has sunken below the Fermi energy. This creates extra transition possibilities and the low-energy peaks for ZrO and HfO are consequently larger and more extended than for TiO. The bands around the Fermi level are all mostly of *d* character. In order to get large interband transitions the *p* bands lying between -6 and -7 eV have to be engaged. For TiO the minimum energy difference between the *p* and unoccupied *d* bands is at Γ, but for ZrO and HfO this *d* band has, as mentioned, sunken below the Fermi energy and so the minimum energy difference occurs a bit away from the center of the Brillouin zone. Just as for the other compounds, the transitions at the higher part of the spectra shown are mainly due to $p \rightarrow d$ transitions. The $s \rightarrow p$ transitions become more important as the energy is further increased.

It is now clear how the main features of the optical properties relate to band filling, anion nuclear charge, and *d*-band width. Increasing the atomic number of the anion causes the Fermi level to move into the group of *d* bands (band filling) and the energy difference between the *p* and *d* bands to increase since the anion nuclear charge is increased. In the case of the carbides, the *p* and *d* band groups are situated almost symmetrically around the Fermi energy. This causes interband transitions at very low energies. For the nitrides and oxides, the energy difference between the Fermi level and the *p* group of bands has to be overcome for the interband transitions to start. This energy difference is a function of anion atomic core charge, and increases consequently as the anion is changed from N to O. The same is true for the positions of the peaks at higher energies. The width of a band *nd* increases with *n*, and so does the dispersion of *d* bands. As we have seen, flat bands give rise to sharp features in σ_1. Thus, the main effect of increasing the *d*-band width is to make peaks in the spectra less pronounced. Finally, the low-energy features in the nitride and oxide spectra depend, as explained, on the detailed band structure in the vicinity of the Fermi energy. In these compounds, the low-energy bumps are due to transitions between *d* dominated bands. Such details are not possible to predict using general concepts such as band filling, *d*-band width, and the like. However, the excellent agreement between calculated and experimental spectra presented in the previous section gives us hope that accurate band-structure calculation can actually reveal these details of the electronic structure.

3. Effect of the Drude parameters

In all metallic compounds, intraband transitions dominate at low energies. The effect of the intraband transitions differs vastly depending on which optical property we look at. For ϵ_2 and σ_1 they are well confined to the low-energy part of the spectra, but for the reflectivity, electron energy loss, refractive indices, and all other quantities where ϵ_1 is included, the effect of the intraband transitions is more complicated. The reflectivity, for instance, is quite insensitive to the relaxation time but very dependent on the plasma frequency. The effect of increased relaxation time is shown in Fig. 10. (Throughout this section, we have chosen to illustrate our discussion using results for ZrN.) A large relaxation time deepens the reflectivity minimum and gives a larger reflectance in the long-wavelength limit. Thus, a monocrystal should have a deeper reflectivity minimum than a thin film with many scattering centers such as grain boundaries and vacancies. Figure 11 makes clear the effect of the plasma frequency. The position of the reflectivity minimum is very sensitive to the value of the plasma frequency. In a model for the intraband transitions more accurate than the Drude

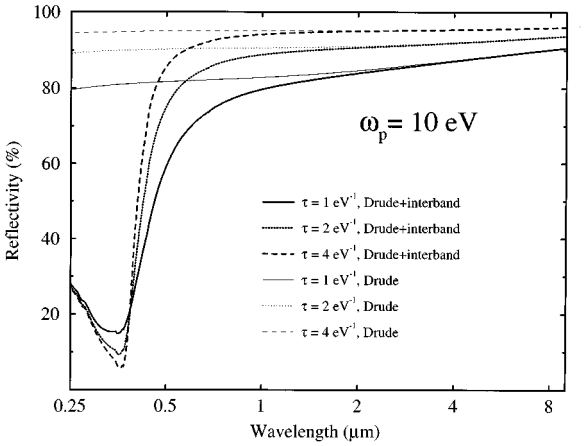

FIG. 10. Illustration of how the reflectivity is affected by the relaxation time τ. The thick lines show the reflectivity when the interband transitions for ZrN are included. The thin lines show how the reflectivity of a pure free electron gas with the same Drude parameters would behave.

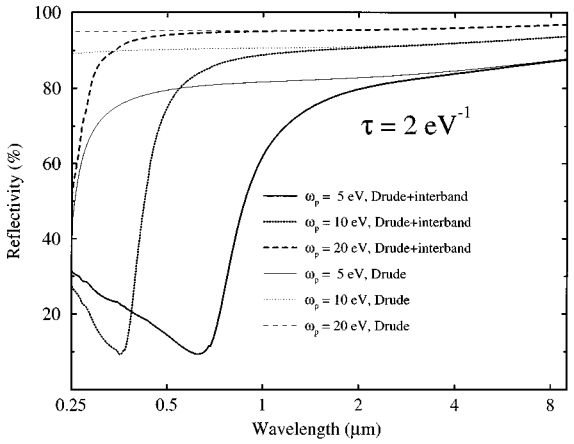

FIG. 11. Illustration of how the reflectivity is affected by the plasma frequency ω_p. The thick lines show the reflectivity when the interband transitions for ZrN are included. The thin lines indicate the reflectance behavior of a pure free electron gas with the same Drude parameters.

model, the parameters vary with energy.[15] This means that ω_p at the reflectivity minimum will not be the same as in the low-energy–high-reflectance region, where the Drude parameters are extracted from experimental data. For this reason, the plasma frequencies used in Fig. 4 are chosen so that the reflectivity minima of the calculated and measured spectra coincide. The plasma frequencies used are generally larger than the experimental ones, suggesting that ω_p is a decreasing function of energy. From Figs. 10 and 11 we can also infer that the free-electron-like region for ZrN starts around 2 μm.

IV. CONCLUSIONS

In conclusion, we have shown that it is possible to calculate the direct interband transitions *ab initio* with high accuracy. This is useful in many ways. A most interesting application of this would be to calculate optical properties of systems where the electronic structure is controversial and compare the results with high precision measurements. We have explained the origin of different structures in the optical spectra and also related the trends in σ_1, caused by changing anion and cation, with general concepts such as band filling, atomic core contraction, and bandwidth. Our interpretation of the origin the structure of σ_1 agrees with previous work[3,11,15,16] done in this area (with one exception, see below) although our analysis is more detailed and concentrated to the region 0–10 eV. The spectrum for TiO in Fig. 5 suggests that this material should have a very tractable solar selectivity since this material is almost free-electron-like up to 6 eV. Unfortunately, because of the vacancy content in real samples, the relaxation time in TiO is very short, which results in unwanted behavior of the reflectivity, see Fig. 10.

The low-energy transitions in the nitrides are often called $d \rightarrow d$ transitions, a name suggesting that quadrupole (or other types of higher-order transitions, e.g., two-step dipole transitions) would actually be of importance, and this interpretation has also been made.[11] There is, however, as our analysis shows, no need to introduce higher-order transitions in order to explain the low-energy bumps in the interband spectra. The pure d orbitals in the free atom are distorted when the atom experiences the potential inside a solid. If one chooses to call this distorted orbital a d orbital, then $d \rightarrow d$ transitions indeed exist. However, the correct mathematical expression of this distorted orbital is a sum of wave functions of different l character. Thus, the distorted orbital will have both s and p as well as d character. In a band picture, this is described as hybridization and mixed l character of the bands. The so-called $d \rightarrow d$ transitions are therefore ordinary dipole transitions in this case.

ACKNOWLEDGMENTS

The authors acknowledge the Optical Materials Group in Uppsala and especially C. G. Ribbing for valuable discussions. A.D. is grateful to the Swedish Research Council for Engineering Sciences for financial support. B.J.and O.E. are grateful to the Swedish Natural Science Research Council for financial support. We also wish to thank the Swedish Materials Consortium No. 9.

[1] P. Hohenberg and W. Kohn, Phys. Rev. **136**, B864 (1964); W. Kohn and L. J. Sham, *ibid.* **140**, A1133 (1965).

[2] S. R. Barman and D. D. Sarma, Phys. Rev B **49**, 16 141 (1994).

[3] S. Gokhale, S. R. Barman, and D. D. Sarma, Phys. Rev. B **52**, 14 526 (1995).

[4] R. Ahuja, O. Eriksson, J. M. Wills, and B. Johansson, Phys. Rev. B **53**, 3072 (1996).

[5] L. E. Toth, *Transition Metal Carbides and Nitrides* (Academic, New York, 1971).

[6] M. Veszelei, K. E. Andersson, and A. Roos, Opt. Mater. **2**, 257 (1993).

[7] V. Ern and A. C. Switendick, Phys. Rev. **137**, 1927 (1965).

[8] A. Neckel, P. Rastl, R. Eibler, P. Weinberger, and K. Schwarz, J. Phys. C **9**, 579 (1976).

[9] P. Blaha, J. Redinger, and K. Schwarz, Phys. Rev. B **31**, 2316 (1985).
[10] D. L. Price and B. R. Cooper, Phys. Rev. B **39**, 4945 (1989).
[11] R. Eibler, M. Dorrer, and A. Neckel, J. Phys. C **16**, 3137 (1983).
[12] C. G. Ribbing (private communication).
[13] M. Veszcelei, K. Andersson, C. G. Ribbing, K. Järrendahl, and H. Arwin, Appl. Opt. **33**, 1993 (1994).
[14] M. Strømme, R. Karmhag, and C. G. Ribbing, Opt. Mater. **4**, 629 (1995).
[15] A. Schlegel, P. Wachter, J. J. Nickl, and H. Lingg, J. Phys. C **10**, 4889 (1977).
[16] B. Karlsson, R. P. Shimshock, and B. O. Seraphin, Solar Energy Mat. **7**, 401 (1983).
[17] D. W. Lynch, C. G. Olson, D. J. Peterman, and J. H. Weaver, Phys. Rev. B **22**, 3991 (1980).
[18] J. M. Wills (unpublished); J. M. Wills and B. R. Cooper, Phys. Rev. B **36**, 3809 (1987).
[19] L. Hedin and B. I. Lundqvist, J. Phys. C **4**, 2064 (1971).
[20] O. K. Andersen, Phys. Rev. B **12**, 3060 (1975).
[21] H. L. Skriver, *The LMTO Method* (Springer, Berlin, 1984).
[22] P. Villars and L. D. Calvert, *Pearson's Handbook of Crystallographic Data for Intermetallic Phases* (American Society for Metals, Metals Park, OH, 1985).
[23] D. J. Chadi and M. L. Cohen, Phys. Rev. B **8**, 5747 (1973); S. Froyen, *ibid.* **39**, 3168 (1989).
[24] P. Drude, Ann. Phys. (Leipzig) **1**, 566 (1900); **3**, 369 (1900).
[25] N. V. Smith, Phys. Rev. B **3**, 1862 (1971).
[26] R. Ahuja, S. Auluck, J. M. Wills, M. Alouani, B. Johansson, and O. Eriksson (unpublished).
[27] See, for example, J. S. Toll, Phys. Rev. **104**, 1760 (1956) and L. D. Landau and E. M. Lifshitz, *Electrodynamics in Continuous Media* (Pergamon, Oxford, 1960).
[28] The relation between the dielectric function and the optical conductivity is ambiguous, see Appendix K in N. W. Ashcroft and N. D. Mermin, *Solid State Physics* (W. B. Saunders, Philadelphia, 1976).
[29] W. Weber, Phys. Rev. B **8**, 5082 (1973).
[30] S. J. Gale and D. G. Pettifor, Solid State Commun. **24**, 175 (1977).
[31] P. Blaha and K. Schwarz, Int. J. Quantum Chem. **23**, 1535 (1983).
[32] W. E. Wall, M. W. Ribarsky, and J. R. Stevenson, J. Appl. Phys **51**, 661 (1980).